

STRINGS IN THE η CARINAE NEBULA: HYPERSONIC RADIATIVE COSMIC BULLETS

A. Y. POLUDNENKO^{1,2}, A. FRANK^{1,2}, S. MITRAN³
Submitted to the Astrophysical Journal

ABSTRACT

We present the results of a numerical study focusing on the propagation of a hypersonic bullet subject to radiative cooling. Our goal is to explore the feasibility of such a model for the formation of “strings” observed in the η Carinae Homunculus nebula. Our simulations were performed in cylindrical symmetry with the adaptive mesh refinement code AstroBEAR. The radiative cooling of the system was followed using the cooling curve by Dalgarno & McCray (1972). In this letter we discuss the evolution and overall morphology of the system as well as key kinematic properties. We find that radiative bullets can produce structures with properties similar to those of the η Carinae strings, i.e. high length-to-width ratios and Hubble-type flows in the form of a linear velocity increase from the base of the wake to the bullet head. These features, along with the appearance of periodic “ring-like” structures, may also make this model applicable to other astrophysical systems such as planetary nebulae, e.g. CRL 618 and NGC 6543, young stellar objects, etc.

Subject headings: circumstellar matter — stars: individual (η Carinae) — stars: mass-loss — ISM: jets and outflows — planetary nebulae: individual (CRL 618)

1. INTRODUCTION

Of the many intriguing questions surrounding the luminous blue variable η Carinae, the origin of the long thin “strings” found in the outer nebular regions remains particularly vexing. First observed by Meaburn *et al.* (1996) and further studied by Weis, Duschl, & Chu (1999) the strings exhibit two remarkable properties: very high values of the length-to-width ratios and the presence of the Hubble-type flow, i.e. linear velocity increase from the base of the strings to their tip. The strings also show a surface brightness decrease toward the string head and the true tips possibly may be invisible in optical wavelengths. These features represent the key challenges that must be met by any model that hopes to offer a successful explanation of the strings’ origin and evolution.

Several models were suggested for the strings including jets (García-Segura *et al.* 1999) and ionization shadows (Soker 2001), see Redman, Meaburn, & Holloway (2002) for a complete discussion of the suggested models. A particularly promising model has been proposed by Redman *et al.* (2002) who suggest that a single hypersonic bullet propagating in the ambient medium is generating the strings observed in the η Carinae nebula. Since the Great Eruption that ejected the main nebula was known to be an impulsive event with most of the mass and momentum directed in the polar directions (Smith *et al.* 2003), and since the strings seem to be coeval with the overall nebula, it is plausible that fragments or bullets were produced in that same event.

In this work we do not address the issue of bullet origin focusing instead on the nature of their evolution and observable properties. In particular, we investigate the feasibility of the Redman *et al.* (2002) model and we address two questions: (1) can a radiatively cooled hypersonic bullet produce structures with large length-to-width ratios, and (2) do such systems exhibit the Hubble-type flow behaviour in their downstream wake.

In Section 2 we briefly discuss the numerical code used, the key dimensionless parameters characterizing the system, and

the setup of the numerical simulation that was carried out. In Section 3 we discuss the results of our numerical study, and in Section 4 we present the conclusions including possible answers to the questions posed above as well as applicability of our results to other astrophysical systems.

2. NUMERICAL STUDY

The simulation presented in this paper was performed with the AstroBEAR code based on the BEARCLAW adaptive mesh refinement package (Mitran 2001; Berger & LeVeque 1998). The code allows for arbitrary levels of refinement within computer memory constraints, as well as adaptive numerics and multiphysics. The Euler hydrodynamic equations with cooling source terms were solved using explicit second-order-accurate scheme. The wave propagation method (LeVeque 1997) was applied with the full nonlinear Riemann solver. An operator split set of ODE’s, describing the source term effects, was solved using the fourth-order-accurate fully implicit Kaps-Rentrop-type scheme (Kaps & Rentrop 1979) (see also (Press *et al.* 1997)).

There are three dimensionless parameters that describe the evolution of the system studied. The first two are the density contrast between the bullet and the ambient medium $\chi_b \equiv \rho_b/\rho_a$ and the Mach number M_b of the bullet velocity at time $t = 0.0$. Those two parameters determine the overall hydrodynamic regime of the system evolution. The third one, the cooling parameter ψ_b , describes the effects of cooling and is defined as

$$\psi_b = \frac{t_{cool}}{t_{hydro}}. \quad (1)$$

Here the hydrodynamic timescale t_{hydro} is defined as the bullet crushing time (or clump crushing time t_{cc} as described by Poludnenko, Frank, & Blackman (2002))

$$t_{hydro} = \left(\chi_b^{1/2} (F_{c1} F_{st})^{-1/2} \right) \frac{2r_b}{v_b}, \quad (2)$$

¹ Department of Physics and Astronomy, University of Rochester, Rochester, NY 14627-0171; wma@pas.rochester.edu, afrank@pas.rochester.edu

² Laboratory for Laser Energetics, University of Rochester, 250 East River Road, Rochester, NY 14623

³ Department of Mathematics, University of North Carolina, CB #3250, Chapel Hill, NC 27599; mitran@amath.unc.edu

where r_b is bullet radius, v_b is bullet velocity, $F_{c1} \approx 1.3$ and

$$F_{st} \simeq 1 + \frac{2.16}{1 + 6.55\chi^{-1/2}}. \quad (3)$$

The two factors F_{c1} and F_{st} relate the unperturbed upstream conditions with the internal bullet post-shock ones and are described in (Poludnenko *et al.* 2002). The interaction of the bullet with the ambient medium launches a shock propagating inside the bullet with the post-shock temperature T_{ps} and ρ_{ps} . The cooling rate Λ_{ps} for such a temperature can be found based on the cooling curve given by Dalgarno & McCray (1972). Thus the cooling timescale is estimated as follows

$$t_{cool} = \frac{T_{ps} - T_{min}}{(\gamma - 1)\rho_{ps}\Lambda_{ps}} km_H, \quad (4)$$

where $T_{min} = 100$ K is the minimum temperature gas can cool down to. The internal bullet post-shock temperature T_{ps} and density ρ_{ps} can be found in the usual manner using the Rankine-Hugoniot relations. T_{ps} and density ρ_{ps} are the functions of the unshocked bullet temperature and density respectively as well as of the internal bullet shock Mach number M_{is} described by the expression

$$M_{is} = M_b (F_{c1} F_{st})^{1/2}. \quad (5)$$

We carried out simulations covering bullet Mach numbers in the range $M_b = 10 - 200$. In terms of the cooling parameter we explored the regimes ranging from the quasi-adiabatic one $\psi_b > 1$ to the strongly cooling one $\psi_b \approx 10^{-5}$. In this paper we will report only on the case that allows us to best address the issues related to η Carinae strings. From our parameter space explorations this turns out to be the case with the strongest cooling $\psi_b = 2.8 \cdot 10^{-5}$. We defer broader conclusions gleaned from the parameter space exploration to a subsequent paper.

Here we present a simulation of bullet propagation where the initial bullet radius is $r_b = 3.0 \cdot 10^{15}$ cm. The initial bullet density is $\rho_b = 10^5 \text{ cm}^{-3}$ in the inner 80% of the bullet radius and in the outer 20% of the radius density is smoothed out through the *tanh*-type function (cf. expression (1) in (Poludnenko *et al.* 2002)). This translates into the initial bullet mass $m_b \approx 0.5 \cdot 10^{-5} M_\odot$. The initial bullet Mach number is $M_b = 20$, or $v_b \approx 235 \text{ km s}^{-1}$. The computational domain is of size $1.8 \cdot 10^{17} \text{ cm} \times 2.4 \cdot 10^{16} \text{ cm}$ or expressed in terms of bullet radii $60r_b \times 8r_b$. The ambient density is $\rho_a = 1000 \text{ cm}^{-3}$ and the ambient temperature $T_a = 10^4 \text{ K}$. It is assumed that initially the bullet is in pressure equilibrium with the ambient material.

The run was carried out in cylindrical symmetry with the x -axis being the symmetry axis. We use an adaptive grid with 4 levels of refinement. This provided a resolution of 128 cells per cloud radius or an equivalent resolution of 1024×7680 cells. Although the above resolution is sufficient to place the simulation in the converged regime in the adiabatic case (Klein, McKee, & Colella 1994), in the cooling case one has to be more precise in one's definition of convergence. Since, as it will be discussed below, the key process in the system is bullet fragmentation via instabilities at the upstream surface, our criterion of convergence was the constancy of the initial fragmentation spectrum. In this sense the above resolution ensured that the instability wavelength, and therefore the number of fragments into which the bullet breaks up, does not change with increasing resolution. On the other hand, it should be mentioned that such resolution might not be sufficient to track the contraction

of each fragment due to radiative cooling to its smallest size defined by the equilibrium between cooling and external heating. Finally, outflow boundary conditions were prescribed on all boundaries.

For the simulation described above the cooling parameter was $\psi_b = 2.8 \cdot 10^{-5}$. The hydrodynamic timescale, i.e. the bullet crushing time, was $t_{hydro} = 2.54 \cdot 10^9 \text{ s} \approx 80.5 \text{ yrs.}$, the cooling timescale was $t_{cool} = 70.9 \cdot 10^3 \text{ s} \approx 19.7 \text{ hours}$. The simulation total run time was $9.49 \cdot 10^9 \text{ s} \approx 251.1 \text{ yrs}^4$. Thus the evolution of the system was in a regime strongly dominated by cooling.

3. RESULTS

3.1. Overall Morphology and Evolution of the System

When the interaction of an inhomogeneity (bullet or clump) proceeds in the adiabatic regime the dominant process defining the evolution of the system is the lateral clump re-expansion (Klein *et al.* 1994; Poludnenko *et al.* 2002). The internal shock compresses the clump and once such compression is completed the re-expansion begins into regions of lowest total pressure, i.e. in the lateral direction. Such re-expansion, acting in combination with instabilities at the upstream clump surface, is responsible for the destruction of the clump. When more than one clump is present, lateral re-expansion also drives interclump interactions via merging and formation of larger structures that subsequently alter the global flow (Poludnenko *et al.* 2002).

The fundamental distinction between the radiatively cooled inhomogeneous systems, including individual bullets, and the adiabatic ones is the minimal role of lateral re-expansion. Instead, the dominant process is the formation of instabilities at the upstream surface of the bullet with a wavelength significantly smaller than the one observed in the adiabatic case. As the bullet begins to drive through the ambient medium, hydrodynamic instabilities (Richtmeyer-Meshkov, Rayleigh-Taylor) produce the initial instability seed. The resulting density variations quickly trigger the onset of thermal instabilities which thereafter become the dominant process responsible for bullet fragmentation. In our simulation such instabilities started developing with a wavelength of about 8 - 10% of the initial bullet radius or $2.4 \cdot 10^{14} - 3.0 \cdot 10^{14} \text{ cm} \approx 16 - 20 \text{ a.u.}$ This initial scale is crucial for subsequent evolution since it determines not only the continuing process of bullet fragmentation but also the structure of the downstream flow. As it was mentioned above, we did not observe any significant changes in the fragmentation spectrum with changing grid resolution, therefore we believe that we observed the true fragmentation spectrum corresponding to the given flow conditions. Of course this conclusion may be altered with fully 3-D simulations. The question of predicting the properties of the initial fragmentation spectrum for the given characteristics of the system is important for the understanding of the physics of radiative hypersonic inhomogeneous systems, however it is outside the scope of the current paper and it will be investigated in the subsequent work.

Since the wavelength of the initial fragmentation spectrum is approximately constant along the bullet radius, the fragments produced by the instability are of different mass with the most massive ones being closest to the symmetry axis and the outermost ones being the lightest. As a result the fragments are "peeled off" from the bullet one by one starting with the outermost ones in radius. Each fragmentation event results in the

⁴ Note that the simulation run time is larger than the age of the η Carinae strings ($\approx 150 \text{ yrs.}$). However, since it is the dimensionless numbers that determine the system evolution, the results can be appropriately scaled to η Carinae conditions. We discuss that in further detail in Section 3.2.

formation of a distinct “ring-like” feature in the bullet wake. The formation of rings is a consequence of the axisymmetry of these simulations. In 3-D it is likely that the rings would themselves fragment (Klein *et al.* 2003; Robey *et al.* 2002).

One noteworthy point is that the evolution of the bullet and its fragments suggests the presence of steady “mass loading” of the downstream flow via the hydrodynamic ablation. Mass loading has been claimed to be an important process in all clumpy hydrodynamic systems (Hartquist *et al.* 1986; Hartquist & Dyson 1988). The extent and nature of such mass loading will be investigated in the subsequent work.

Figure 1 shows the computational domain at time $t = 251.1$ yrs. In Figure 1a the synthetic Schlieren image (gradient of the density logarithm) is shown illustrating the shock and vortex sheet structure in the flow. Figure 1b shows the synthetic observation image of the computational domain. Since our simulation did not track the full ionization dynamics of the flow, the image represents the total radiative energy losses summed along each ray. The 2D distribution of the state vector obtained in the simulation was extended using cylindrical symmetry to a $2048 \times 2048 \times 7680$ cells uniform grid 3D data cube. Thus the synthetic observation image represents the 2D projected distribution of the logarithm of the emissivity I integrated in the z-direction according to the formula

$$I_{ij} = \sum_k n_{ijk}^2 \Lambda_{ijk}(T_{ijk}), \quad (6)$$

where i , j , and k are the cell indices in the x-, y-, and z-direction respectively, and the cooling rate $\Lambda(T)$ here, as well as in the simulation, was determined based on the cooling curve described by Dalgarno & McCray (1972).

There are several ring-like structures in Figure 1 in the bullet wake. These result from the fragmentation events mentioned above. The most prominent ring occurs at the distance of $\approx 1.38 \cdot 10^{17}$ cm from the bullet head (ring 1) with the width of $\approx 2.94 \cdot 10^{16}$ cm ≈ 1965 a.u. which is the widest part of the bullet wake. In Figure 1b several other bright rings, resulting from fragmentation events, are visible closer to the bullet head. They gradually increase in radius further downstream with the radius of the largest ring (ring 2), located at the distance of $\approx 5.8 \cdot 10^{16}$ cm from the bullet head, being $\approx 1.82 \cdot 10^{16}$ cm ≈ 1216 a.u. Note that the width of the bullet wake stays practically constant, increasing only slightly, for a distance of $\approx 8.0 \cdot 10^{16}$ cm ≈ 5350 a.u. from ring 2 to ring 1. Thus in our simulations the length-to-width ratio of the bullet wake is 6.1–9.9 and the bullet wake width is 4–6.5 times larger than the width of String 5 while they share the same length. Note also that the width of the bullet head is only $\approx 1.05 \cdot 10^{15}$ cm ≈ 70 a.u. We followed the simulation beyond the time $t = 251.1$ yrs, shown in Figures 1 and 2, up to the time $t = 300.8$ yrs. and we did not observe any appreciable changes in the aforementioned values of the length-to-width ratio.

The second process that determines the structure of the flow in the wake is gas re-expansion into the cavity excavated by the bullet. The highest temperature reached by gas in the system is at the tip of the central bullet fragment and is about $3.5 \cdot 10^5$ K. Gas passing through the bullet bowshock cools down very rapidly, weakening the bowshock and making it more oblique, which in its turn prevents further heating of the ambient gas. As it can be seen in Figure 1a, the bowshock practically disappears half-way downstream from the bullet head. Beyond the turbu-

lent region immediately behind the bullet head and in between the stripped bullet fragments, the gas tends to re-expand essentially at the sound speed of the ambient gas and fill the cavity. Such re-expansion causes gas to rebound on the axis resulting in a reflected shock. The effect of this shock can be seen in Figure 1a around the symmetry axis as a complex shock region that is narrower than the bowshock.

Note, that in Figure 1b the surface brightness of the system increases toward the bullet head. This differs from the surface brightness behaviour observed in the η Carinae strings. As was noted by Weis *et al.* (1999) the string surface brightness decreases toward the head so that the true string tip might not even be detected. Recall, however, that Figure 1b is not a true synthetic observation image in a certain line but rather a projected map of total radiative energy losses in the system. In addition illumination by stellar photons is not included in our calculation. Thus in the simulation the bullet head and its vicinity, where the density and temperature are highest so that $n^2\Lambda(T)$ are large, appear brightest. In reality gas in the bullet head and near it may be too hot to be visible optically as was suggested by Redman *et al.* (2002). In our further work we plan to include tracking of full ionization dynamics that will allow us to produce true synthetic observation images in a particular emission line or a combination of lines.

3.2. Velocity Distribution and Hubble-type Flow

Another key property of the strings is the presence of Hubble-type flows in the bullet wake. The left panel of Figure 2 shows the distribution of the total velocity $v_{tot}(x)$ along the symmetry axis of the bullet/wake as a function of distance from the bullet head. The linear velocity decrease from the maximum value of 210 km s^{-1} from head to base is clear aside from some minor fluctuations arising due to the unsteadiness of the downstream flow⁵. Note that very little deceleration of the bullet head has occurred. Given that the initial bullet velocity is 235 km s^{-1} we see that after 251.1 yrs., in which the bullet material traveled the distance of $1.8 \cdot 10^{17}$ cm ≈ 0.058 pc, the bullet material lost only $\approx 10\%$ of its original velocity. That is due to the fact that the central fragment retains most of the original bullet mass while it has a rather small cross-section due to the cooling-induced contraction.

Weis *et al.* (1999) quote a velocity slope in the η Carinae strings ranging from $2590 \text{ km s}^{-1}\text{pc}^{-1}$ (String 5) to $3420 \text{ km s}^{-1}\text{pc}^{-1}$ (String 2). In our simulation we find a velocity slope of $3600 \text{ km s}^{-1}\text{pc}^{-1}$ which is about 5% - 40% higher. Note, that the length of String 5 is practically equal to the distance over which we allowed the bullet to propagate, however String 2 is about 25% shorter (Weis *et al.* 1999).

One should be cautious, however, in directly comparing the total velocity distribution shown in the left panel of Figure 2 to the observationally determined velocity distributions in the strings of η Carinae (cf. Figure 6 in (Weis *et al.* 1999)). Quantities, more closely resembling the ones that are obtained observationally, should be employed in order to make the comparison between the numerical results and observations relevant. For example, one can create emissivity-weighted total velocity $v_{emis}(x)$ maps of the flow. Distribution of such a quantity along the x-axis is shown in the right panel of Figure 2. $v_{emis}(x)$ was

⁵ It should be noted that we observed similar behaviour of the total velocity distribution in other systems with the cooling parameter up to $\psi_b \approx 0.25$. For systems approaching the adiabatic regime with $\psi > 1.0$ the velocity distribution takes a more complicated form.

obtained according to the formula

$$v_{tot}(x) = \frac{\sum_j n_j^2 \Lambda_j v_j}{\sum_j n_j^2 \Lambda_j} \approx \frac{\int_{y_{min}}^{y_{max}} n^2(x, y) \Lambda(x, y) v_{tot}(x, y) dy}{\int_{y_{min}}^{y_{max}} n^2(x, y) \Lambda(x, y) dy}, \quad (7)$$

where i and j are the cell indices in the x - and y -directions, v_j is the total velocity in the cell j , and in the summation in the numerator we included only the cells with non-zero total velocity. The distribution of this quantity is significantly more noisy than the total velocity cross-cut. However, the local maxima of $v_{emis}(x)$ roughly tend to fall on the same line as that in the previous figure giving some indication of the presence of the Hubble-type flow.

The distance traveled by the bullet in our simulation is practically equal to the length of String 5 and is factors of 1.5–3.0 shorter than the rest of the strings (except for String 2) (Weis *et al.* 1999). If we assume that the true length of strings is not their observed length but rather the distance of the tip from the star, than the η Carinae strings are the factors of 3.2–5.56 longer (Weis *et al.* 1999) than the computational domain in our simulation. However, the kinematic age of the bullet in our simulation is about 67% larger than that of the η Carinae strings: 251.1 years vs. 150 years. This indicates that in our simulation the bullet velocity was approximately a factor 2.5–5.0 (or a factor 5.35–9.3 if we assume that the string base is located near the central star) smaller than in the case of η Carinae strings, i.e. the bullet velocity should be 590–1175 km s⁻¹ (or 1260–2185 km s⁻¹) with respect to the central star. An increased bullet velocity would decrease the width of the bullet wake and increase the length-to-width ratio making a better match between our simulations and the strings of η Carinae. However, a significant increase in velocity, and therefore Mach number, results in much higher temperatures in the bullet wake and the bow shock. That, in turn, increases the cooling parameter ψ_b , eventually sending the system into the adiabatic regime which no longer exhibits the high length-to-width ratio of the wake and the Hubble-type downstream flow⁶. The easiest way to reconcile the need for the significantly higher bullet velocity, required in order to obtain the correct kinematic age, with the need for the relatively low post shock temperatures, required to decrease the bullet wake width, is to embed the bullet in the ambient flow that itself moves with significant speed relative to the central star. There is some observational evidence for the presence of such high velocity ambient flow (Weis, Duschl, & Bomans 2001). For example, string 1 may be embedded in the material moving with velocity ≈ 500 –600 km s⁻¹ with respect to the central star, whereas the maximum velocity of the string material is ≈ 995 km s⁻¹ (Weis *et al.* 1999).

4. CONCLUSIONS

In this paper we have presented a numerical study of a hypersonic radiative cosmic bullet in an attempt to model the strings

observed in the η Carinae Homunculus nebula. Our simulations follow from the discussion by Redman *et al.* (2002).

Our principal conclusions are as follows: (1) hypersonic radiative bullets are capable of producing structures with high length-to-width ratios (between 6 and 10 for our study); (2) the dominant process responsible for bullet destruction is instability formation at the bullet upstream interface leading to separate fragmentation episodes; these result in the formation of periodic “ring-like” structures in the bullet wake; (3) the simulations do show the presence of Hubble-type flows along the axis in the bullet wake in terms of a linear decrease of the total velocity downstream from the bullet head. How these flows appear observationally remains an open question.

Thus we conclude that the bullet model appears as a good candidate for the strings of η Carinae, though further work is needed. If this model finds continued success then theorists will confront the issue of how such high velocity bullets are generated, i.e. at the star or at larger distances. Confirming the existence of such bullets may be helpful in determining the nature of the processes, occurring within the star, which were part of its various eruptions.

The astrophysical applicability of the model, discussed in this paper, might extend beyond the η Carinae strings. One of the most spectacular examples of nebular systems with long thin structures is the protoplanetary nebula CRL 618 and, in particular, its shocked lobes. The most prominent features of the lobes are the periodic rings similar to the ones present in our simulation. As it was discussed, such rings arise naturally as a consequence of the bullet fragmentation events. There is also some evidence for the velocity increase in the lobes from the base to the tip (Sánchez Contreras, Sahai, & Gil de Paz 2002). Other examples include, but are not limited to, other planetary nebulae, e.g. strings in NGC 6543 (Weis *et al.* 1999), HH objects, etc.

Further developments of the model should include the study of the details of the formation of the initial fragmentation spectrum, investigation of the importance of mass-loading due to the ablation of the bullet head and bullet fragments, and inclusion of more realistic description of ionization dynamics and radiative cooling in the system. The latter will allow us to produce more realistic synthetic observation images and synthetic spectra for better comparison with observational data.

This work was supported in part by the NSF grant AST-9702484, NASA grant NAG5-8428 and the Laboratory for Laser Energetics under DOE sponsorship.

The most recent results and animations of the numerical experiment, described above as well as the ones not mentioned in the current paper, can be found at www.pas.rochester.edu/~wma.

REFERENCES

- Berger, M. J., LeVeque, R. J. 1998, SIAM J. Numer. Anal., 35 (6), 2298
 Dalgarno, A., McCray, R. A. 1972, ARA&A, 10, 375
 García-Segura, G., Langer, N., Różyczka, M., Franco, J. 1999, ApJ, 517, 767
 Hartquist, T.W., Dyson, J.E. 1988, Ap&SS, 144, 615
 Hartquist, T.W., Dyson, J.E., Pettini, M., Smith, L.J. 1986, MNRAS, 221, 715
 Kaps, P., Rentrop, P. 1979, Numerische Mathematik, 33, 55
 Klein, R. I., Budil, K. S., Perry, T. S., Bach, D. R. 2003, ApJS, 583, 245
 Klein, R.I., McKee, C.F., Colella, P. 1994, ApJ, 420, 213
 LeVeque, R. J. 1997, J. Chem. Phys., 131, 327
 Meaburn, J., Boumis, P., Walsh, J. R., Steffen, W., Holloway, A. J., Williams, R. J. R., Bryce, M. 1996, MNRAS, 282, 1313
 Mitran, S. M. 2001 <http://www.amath.unc.edu/Faculty/mitran/bearclaw.html>.
 Press, W. H., Teukolsky, S. A., Vetterling, W. T., Flannery, B. P. 1997, Numerical Recipes in Fortran 77: The Art of Scientific Computing, Vol. 2, (2nd ed.; Cambridge University Press)
 Poludnenko, A. Y., Frank, A., Blackman, E. G. 2002, ApJ, 576, 832

⁶ We observed that effect in a simulation of Mach 200 bullet propagation. The cooling parameter for that case was $\psi_b = 3.7$. We do not discuss this simulation in this paper however its animation can be accessed at the web site mentioned in the acknowledgment section.

Redman, M. P., Meaburn, J., Holloway, A. J. 2002, MNRAS, 332, 754
Robey, H. F., Perry, T. S., Klein, R. I., Kane, J. O., Greenough, J. A., Boehly, T.
R. 2002, Phys. Rev. Lett., 89 (8), 085001
Sánchez Contreras, C., Sahai, R., Gil de Paz, A. 2002, ApJ, 578, 269

Smith, N., Gehrz, R. D., Hinz, P. M., Hoffmann, W. F., Hora, J. L., Mamajek,
E. E., Meyer, M. R. 2003, ApJ, 125, 1458
Soker, N. 2001, A&A, 377, 672
Weis, K., Duschl, W. J., Bomans, D. J. 2001, A&A, 367, 566
Weis, K., Duschl, W. J., Chu, Y.-H. 1999, A&A, 349, 467

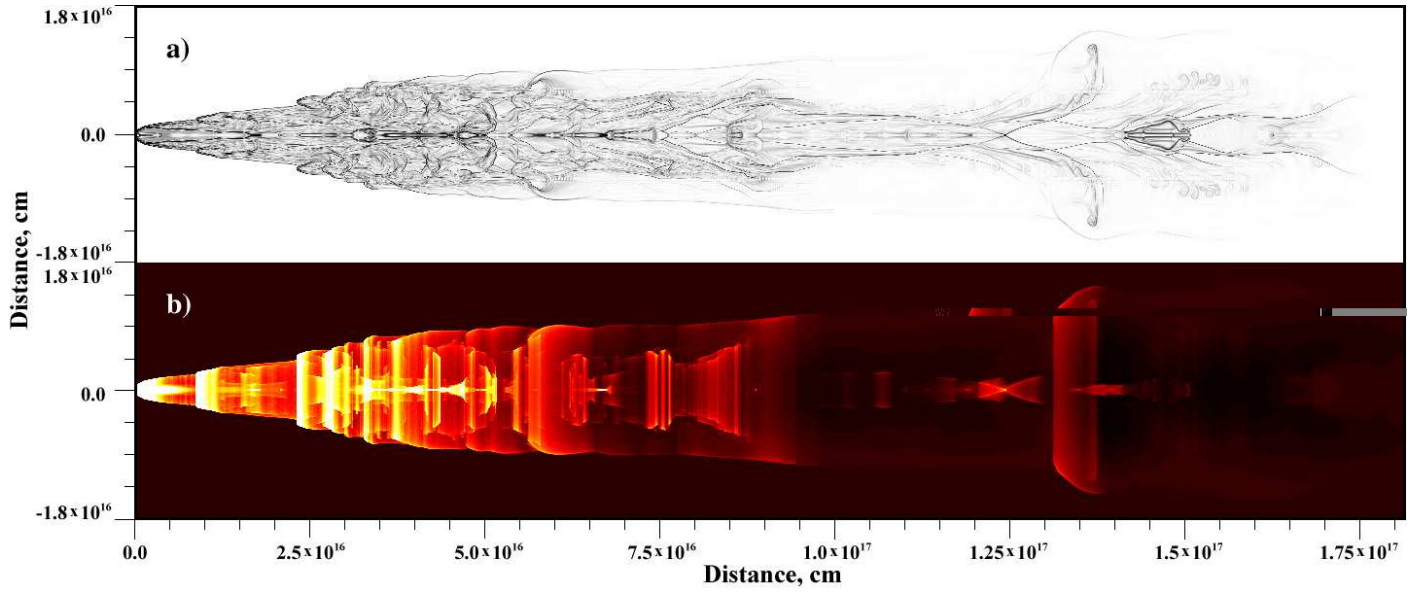


FIG. 1.— a) Synthetic Schlieren image of the computational domain at time 251.1 yrs. Shown is the gradient of the density logarithm. b) Synthetic observation image of the computational domain for the same time as in a) (see text for the detailed description). Note the periodic ring-like structures in the domain resulting from individual fragmentation episodes.

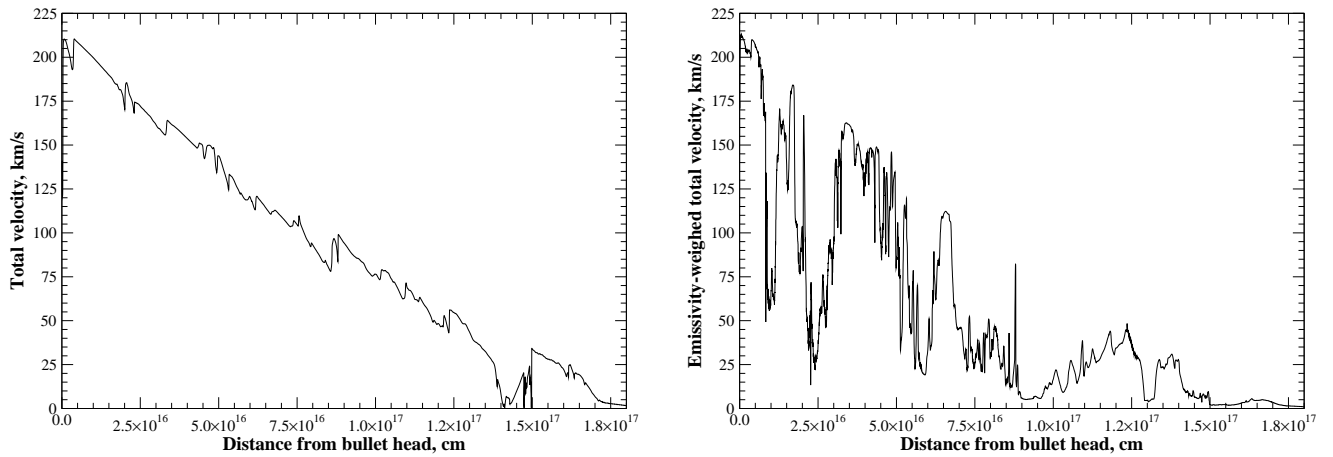


FIG. 2.— *Left*: distribution of total velocity along the symmetry axis of the bullet at the time 251.1 yrs. (same time in the simulation as the one shown in Figure 1). *Right*: distribution of the emissivity-weighted total velocity in the system at the same time (see text for the detailed description).